NEARSHORE COASTAL PROCESSES ADJACENT TO A TIDAL INLET

Thomas O. Herrington[1], Associate Member, ASCE, Michael S. Bruno[2], Member, ASCE, Majid Yavary[3], Student Member, ASCE, and Kelly L. Rankin[1]

Abstract

Two tidal inlets with strikingly different physical characteristics have been investigated through an analysis of multi-year beach survey results and field investigations of the nearshore wave and current structure adjacent to the inlets. The survey results indicate that the downdrift shoreline adjacent to both inlets is dominated by persistent inlet directed currents, which run counter to the net sediment transport direction. The two wave and current studies differed in both their spatial and temporal resolution, requiring the use of separate analysis techniques to determine the forcing mechanisms responsible for the observed inlet directed currents. The two analysis techniques produced similar results which indicate that tidal-induced circulation generates the persistent nearshore current structure. Episodic wind-generated currents and nonlinear wave and current interactions were found to reach the same order of magnitude as the tide-induced currents, and could either enhance or reverse the observed nearshore current structure.

Introduction

It has been observed that in the vicinity of coastal inlets, complex interactions between tidally-driven currents and shoreward propagating waves produce unique wave transformation patterns that in turn give rise to sediment transport characteristics that differ greatly from adjacent shoreline areas. Shorelines adjacent to tidal inlets are subjected to a number of spatially- and temporally-varying forces, such as tidal motions, wind stress, wind waves, swell, freshwater inflow, density driven circulation, and variations in atmospheric pressure. Although much has been learned about the nature of these interactions, and their impact on sediment transport, there are very few comprehensive

[1] Res. Asst. Prof, Dept. of Civ.,Envir.,and Ocean Engrg., Stevens Inst. of Tech., Hoboken, NJ 07030
[2] Prof., Dept. of Civ.,Envir.,and Ocean Engrg., Stevens Inst. of Tech., Hoboken, NJ 07030
[3] Grad. Student, Dept. of Civ.,Envir.,and Ocean Engrg., Stevens Inst. of Tech., Hoboken, NJ 07030

measurements in dynamically-active regions such as tidal inlets that would allow one to examine the response of the shoreline to the multitude of forcing mechanisms.

Two recent multi-year shoreline monitoring studies in New Jersey have focused on the impact of tidal inlets on shoreline evolution. Each study included an analysis of long-term beach profile surveys and short-term wave and near-bottom current measurements. The initial study was conduced at Townsends Inlet in Avalon, New Jersey (Figure 1). Townsends Inlet is a relatively unimproved inlet approximately 500 m wide, stabilized by a 180 m long stone jetty located on the south side of the channel. Analysis of 10 years of beach profile data at the site indicate that the sediment transport pattern adjacent to the inlet is opposite the net southerly transport direction along this reach of coast (Farrell et. al., 1995). A second multi-year study was conducted 110 km north of Townsends Inlet at Manasquan Inlet, New Jersey (Figure 1). This improved inlet has a 122 m wide entrance channel protected by two 400 m long parallel stone jetties. Analysis of 3 years of beach profile data north of the inlet also indicates the presence of a localized reversal in the net northerly sediment transport direction.

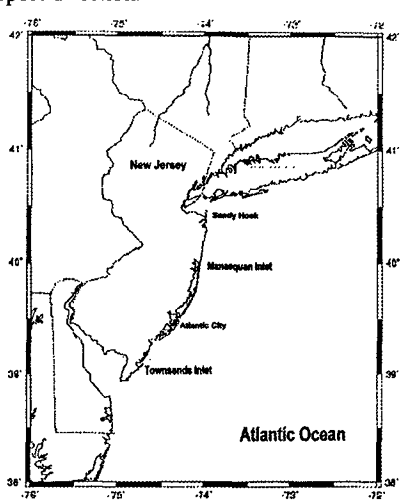

Figure 1. Location Map

Field Measurements and Analysis

Manasquan Inlet

Repetitive, high-resolution cross-shore beach profile measurements, obtained over a period of 3 years along the shoreline north of the Manasquan Inlet, indicated the presence of an area of localized erosion between 250 m and 750 m from the inlet. This erosion hot spot is characterized by a 38 m recession in the position of the mean low water line relative to the shoreline position 100 m to the north and south.

In an effort to identify the possible causes for the area of accelerated erosion, a comprehensive field study was conducted in and around Manasquan Inlet on 17 April 1996. Wave and near-bottom current measurements (1 m above the seabed) were obtained during the one day study by 3 bottom mounted InterOcean Systems S4 electromagnetic current meters fitted with high resolution pressure, temperature and conductivity sensors. Two of the bottom mounted gauges were located seaward of the inlet; S1 approximately 700 m offshore in a water depth of 13 m mean sea level (MSL), and S2 approximately 360 m offshore at a depth of 11 m MSL (Figure 2). The third gauge was located 385 m offshore of the erosion hot spot, 550 m north of the inlet, in 9.5 m of water MSL. All of the gauges were configured to sample continuously at 2 Hz and internally record the measured parameters over the duration of the study. In addition to the near-bottom point measurements, the spatial distribution of both the horizontal and vertical current structure was obtained through the use of a towed Acoustic Doppler Current Profiler (ADCP) (Bruno, et. al., 1998). The ADCP provided measurements of the top to bottom current profile along a series of transects that spanned the inlet throat, the adjacent shorelines to the north and south, and across the ebb shoal out to a water depth of 13.5 m MSL. The position of the ADCP during each transect was determined continuously using a shore-based surveying total station equipped with an Electronic Distance Meter (EDM), which obtained angle and distance measurements to a reflective prism mounted on the boat. Meteorological conditions (wind speed and direction) during the study were obtained by an anemometer located at the eastern tip of the southern inlet jetty, 10 m above the water surface.

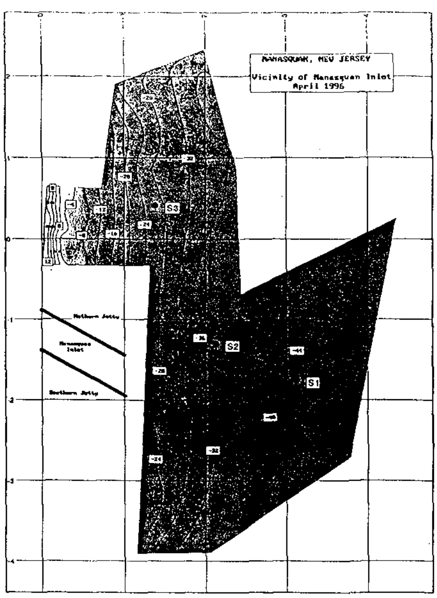

Figure 2. Location of bottom mounted S4 meters. Depth contours in feet, MSL

The high-resolution current study spanned both the ebb and flood portions of a spring tidal cycle with a predicted range of 1.5 m. The meteorological and oceanographic conditions over the duration of the study are presented in Table 1.

Table 1. Measured Physical Conditions, 17 April 1996

Time (GMT)	Wind Speed (m/s)	Wind Dir. (N)	Gauge	Water Depth (m)	Wave Height Hmo (m)	Wave Period Tp (s)	Wave Dir. (N)	Salinity (ppt)	Temp. (C)
1540 (Ebb)	10	303	s1	13.29	0.94	9.5	55.7	31.2	5.0
			s2	11.45	1.00	9.0	50.0	31.5	5.0
			s3	9.64	0.91	9.1	82.0	31.6	5.5
1900 (Slack)	10	303	s1	13.12	0.95	9.1	60.5	31.5	5.0
			s2	11.30	0.65	9.1	57.6	31.8	5.0
			s3	9.53	0.81	9.8	80.0	31.8	4.8
2040 (Flood)	10	303	s1	13.70	0.88	8.0	47.5	31.5	5.0
			s2	11.89	0.74	9.3	59.0	31.8	5.0
			s3	10.11	0.90	10.2	81.0	32.5	4.5

Throughout the study period the wind was directed offshore toward the southeast at 10 m/s, significant wave heights ranged from 0.74 to 1.00 m propagating from the northeast with an average peak period of 9.2 s.

The high-resolution current survey spanned both the flood and ebb portions of the tidal cycle. Each round of transects was completed in approximately 30 minutes in order to provide a nearly synoptic measurement of the current pattern at various phases of the tide. Figure 3a illustrates the near-surface current distribution at peak ebb tide (1500 GMT). The measurements indicate a strong flow exiting the inlet, with near-surface currents exceeding 1 m/s. The near-bottom current structure exiting the inlet at peak ebb (Figure 3b) indicates a reduction in the current velocity to between 0.33 and 0.55 m/s. In contrast to the strong jet-like outflow on the surface, the weaker near-bottom currents are directed inshore toward the inlet. Interestingly, in both the surface and bottom currents there is evidence of inlet-directed return flows along the transects north and south of the inlet. This return flow is reflected in the near-bottom current measurements obtained by the three S4 gauges. Figure 4 illustrates the time history of the north-south component of the 9 minute average near-bottom velocity at each gauge (north is positive). Note that although the two gauges located seaward of the inlet , S1 and S2, recorded a reversal in current direction as the tide turned from flooding to ebbing, the nearshore gauge, S3, recorded a nearly constant southward directed near-bottom motion.

In an effort to gain some insight into the forcing mechanism responsible for the observed persistent inlet directed near-bottom flow seaward of the erosion hot spot, an order of magnitude comparison of the measured forcing mechanisms can be conducted. The physical forcings of interest include, wave-induced longshore transport, wind-generated currents, and inlet-induced circulation.

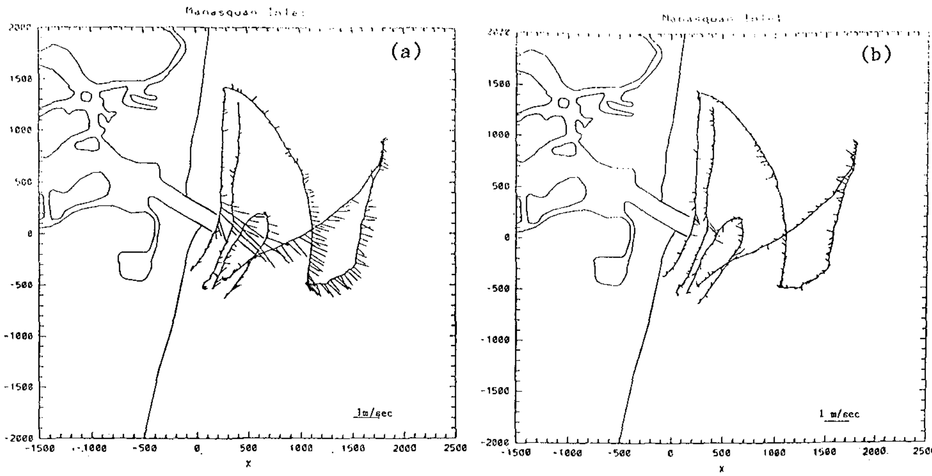

Figure 3. Spatial Current Distribution at 1500 GMT: (a) Near-Surface; (b) Near-Bottom

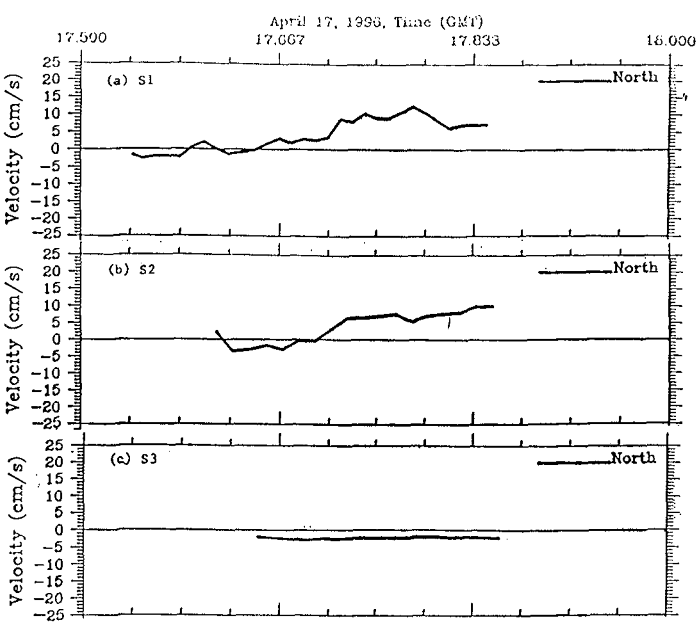

Figure 4. Average (9 min.) Near-Bottom Current: (a) S1; (b) S2; (c) S3

Utilizing the breaking criteria, $h_b = 1.28\ H_b$, where H_b, is the wave height at breaking and h_b, is the water depth at breaking, the location of the average location of the surfzone on 17 April, 1996 was in 1.1 m of water MSL, placing meter S3 approximately 305 m seaward of the surfzone. Based on Longuet-Higgins' (1970) formulation, the wave-induced longshore current 300 m seaward of the surfzone is negligible.

The wind-generated current at the surface of the water column can be estimated as 3 % of the wind speed 10 m above the water surface (U_{10}). In shallow water the wind-generated transport is essentially in the direction of the wind stress (Pond and Pickard, 1983). Assuming a logarithmic decay of the surface current with depth, the current generated by the wind stress 1 m above the bottom can be expressed as:

$$V_0 - V_1 = \frac{u_*}{\kappa} \ln\left(\frac{h}{z}\right) \tag{1}$$

where V_0 is the surface current ($= 0.03U_{10}$), V_1 is the current speed 1 m above the bottom, u_* is the current shear velocity, κ is von Karman's constant ($\kappa = 0.4$), h is the water depth, and z is the distance of the current meter above the bed. The current shear velocity is calculated as:

$$u_* = \sqrt{\frac{\tau}{\rho}} \tag{2}$$

where the bottom shear stress, τ, is given as:

$$\tau = \frac{1}{2}\rho C_f V_0^{\,2} \tag{3}$$

In equation 3, ρ is the water density and C_f is the current friction factor. Substituting equations (2) and (3) into (1) and rearranging:

$$C_f = \left(\frac{2}{V_0}\right)\left(\frac{\kappa(V_0 - V_1)}{\ln(h/z)}\right)^2 \tag{4}$$

Utilizing the ADCP current profile data, equation 4 can be used to directly solve for the current friction factor, C_f. Table 2 lists the near-surface and near-bottom current velocities, and the calculated friction factor, C_f, measured within 300 m of gauge S3 at peak ebb (1500 GMT) on 17 April 1996.

Table 2. Measured Current Shear within 300 m of gauge S3 at 1500 GMT

Point	Wind Speed (m/s)	Wind Dir. (N)	Water Depth (m)	Surface Current (m/s)	Bottom Current (m/s)	Current Shear, u_* (m/s)	Shear Stress, τ (kg/ms^2)	Friction Factor C_f
1	10	303	9.64	0.20	0.05	0.026	0.72	0.04
2	10	303	9.64	0.11	0.02	0.016	0.26	0.04
3	10	303	9.64	0.09	0.00	0.016	0.26	0.06
4	10	303	9.64	0.05	0.00	0.009	0.08	0.06
5	10	303	9.64	0.21	0.00	0.037	1.41	0.06
6	10	303	9.64	0.27	0.11	0.028	0.82	0.02

Substituting the data obtained at peak ebb, $h = 9.64$ m, $U_{10} = 10$ m/s, $z = 1$ m, $\rho = 1026.9$ kg/m^3, and the average $C_f = 0.05$, into equations (1) through (3) and solving for V_l, yields a near-bottom wind-generated velocity of 3.1 cm/s directed 123° from North. Decomposing the current vector into north and east components gives an alongshore wind-generated current component of 1.7 cm/s to the south.

Joshi and Taylor (1983) analyzed the alongshore and cross-shore velocity components induced by the entrainment of water into nonbuoyant tidal jets issuing into water of constant depth with arbitrary bottom friction. The potential motion induced by an ebbing tidal jet is modeled as a series of sink singularities which constitute elementary solutions to Laplace's equation:

$$\nabla^2 \psi = 0 \tag{5}$$

where ψ is the two dimensional stream function $\psi(x,y)$. Analytic solutions for the jet-induced circulation are obtained by relating the sink strength to the inlet characteristics. These characteristics and the values for Manasquan Inlet include inlet half-width, b_0=61 m, mean channel depth, h_0=3.05 m, inlet throat cross-sectional area. A_c=366 m^2, average velocity over the throat area, u=1.0 m/s, length of inlet channel or jetties, a=400 m, the Darcy-Weisbach friction factor, f= 0.043 the Chezy coefficient, C=42.82 m$^{1/2}$/s, and Manning's n= 0.028.

A series of nondimensional solution curves are presented to determine V, the ratio of alongshore velocity to inlet velocity, based on ζ, the ratio of distance alongshore from the inlet to inlet half width. Solution curves are given for various combinations of dimensionless jetty length, $A=a/b_0$, and dimensionless friction parameter, $\mu = fb_0/8h_0$. For the Manasquan Inlet, $A = 6.5$ and $\mu = 0.107$. From the solution curves presented in Figure 12 (Joshi and Taylor, 1983), the predicted alongshore current 550 m north of the inlet, due to steady potential motion induced by the tidal jet alone, is 1.04 cm/s.

Townsends Inlet

A seven-day time series of wave and near-bottom current measurements were obtained 60 m inshore of the western edge of the main ebb channel of Townsends Inlet, Avalon, New Jersey, in September, 1993 (Figure 5). The wave and current meter was mounted 1 m above the sea bed, 180 m south of the southern inlet jetty, in a mean water depth of 3.0 m MSL. In this configuration the meter was exposed to both nearshore wave and current action as well as strong tidal currents. The meter was initialized to provide measurements of the pressure and two orthogonal components of velocity at 2 Hz over 9 minute burst samples, at one hour intervals.

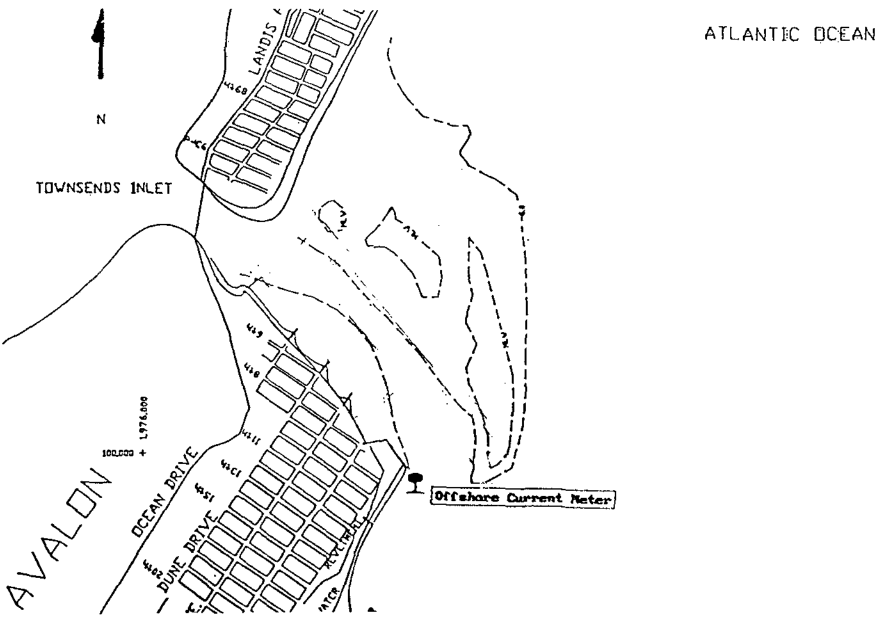

Figure 5. Townsends Inlet. Location of channel and shoals indicated by dashed line.

The measured time series is presented in Figure 6. The tidal elevation record is plotted in the upper panel, followed by the surface wind observations from Atlantic City, (located 45 km north of the inlet), the measured significant wave height ($H_s=4(m_0)^{1/2}$), the peak wave direction, and the 8.5 minute average current measured 1 m above the bottom.

All of the recorded vectors were decomposed into shore-parallel and cross-shore components. Since the axis of the ebb channel of the inlet lies on a bearing of 0° Magnetic North (MN), all of the recorded directions are reported relative to Magnetic North. Thus, shore-parallel components are parallel to the axis of the inlet channel and cross-shore components are perpendicular to the inlet channel. Positive values of the shore-parallel and cross-shore components are directed to magnetic north and east, respectively. Directions are given as the direction of propagation (i.e. a shore-parallel wind of -5 m/s is a wind directed from the north). The x-axis is scaled in tenths of days Eastern Daylight Savings Time (EDT) so that 20.5 would represent the 20th day of the month at 1200 hours.

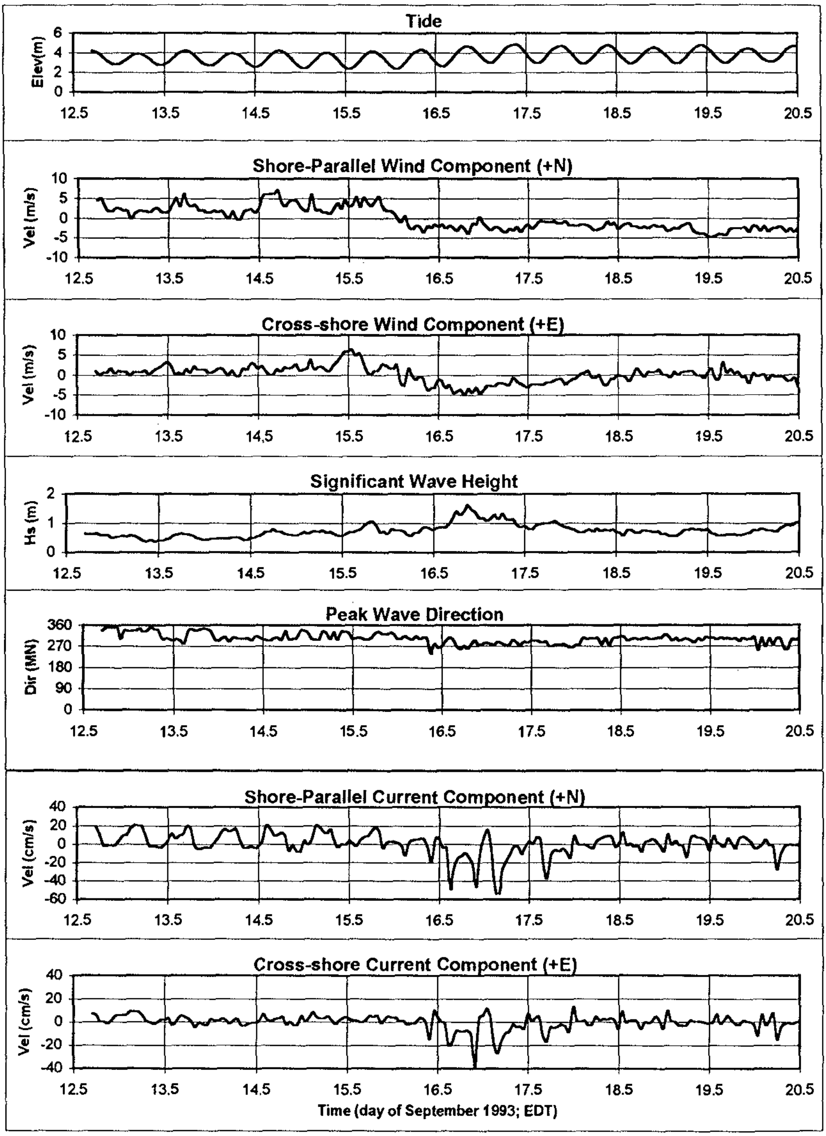

Figure 6. September, 1993 Observations at Townsends Inlet

The energy density spectra for the tidal elevation and shore-parallel component (U-Comp) of velocity is presented in Figure 7. Energy density spectra were calculated for the zero mean records of tidal elevation and the shore-parallel current component for the 7 day data set. The time series were divided into five 64 hour data segments and ensemble averaged with 50% overlap, providing spectral estimates with 10 degrees of freedom and a 95% confidence interval of 25 to 150 percent of the estimates. Examining Figure 7, two peaks are evident in the tidal elevation energy density, one centered at the semidiurnal frequency (0.08 cph) and one centered at a frequency of 0.02 cph. Three peaks in kinetic energy are present in the shore-parallel velocity component. Peaks of equal magnitude (0.175 $(m/s)^2s$) are centered at 0.02 cph and the semidiurnal tidal frequency and a lesser peak of 0.13 $(m/s)^2s$ is centered at a frequency of 0.16 cph.

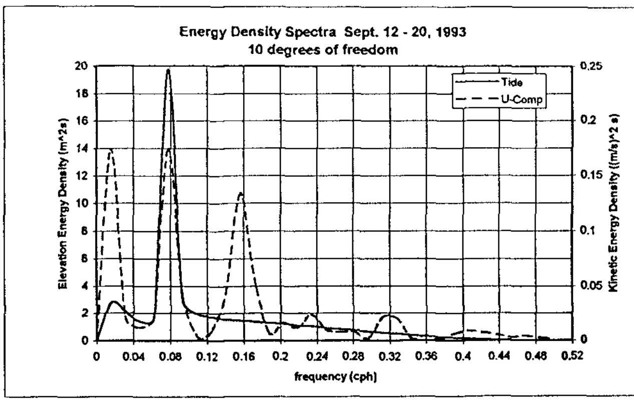

Figure 7. Elevation and Kinetic Energy Density

In an effort to determine the forcing mechanisms responsible for the observed energy density distributions, a multivariable polynomial autoregressive analysis with exogenous variables (PARX) model was utilized to produce empirical fits to the measured nearshore current data. The analysis technique decomposes the measured time series data into a multivariate data set which is utilized to predict one measured variable based on a polynomial function of the remaining variables (see Herrington and Bruno, 1998). Utilizing the six parameters measured, water elevation, h, wave amplitude, a, shore-parallel wave number, k_x, wave frequency, ω, shore-parallel wind speed, W, and the time rate of change of shore-parallel wind speed, dW/dt, a PARX model was developed to predict the measured shore-parallel current velocity. The empirical equation developed by the PARX model to predict the shore-parallel component of velocity, U_{SP}, is

$$U_{SP} = K_W + K_{dW} + K_{AH} + K_K \tag{6}$$

where

$$K_W = [\,0.015157(\omega^2 / W_{t-1}) - 0.0016022\, h^2_{t-2} W_{t-1}\,] + [\,0.13338\, a^2 + 0.011704\, \omega_{t-1} + 0.00058704 /(k\, W^2)]\, W$$

$$K_{dW} = [0.0020512\,(\, dW/dt\,)/k - 0.0017450\,(\, dW/dt\,)_{t-1}/k_{t-1} - 0.0025645\, k_{t-1}/(dW/dt\,)_{t-2}]$$

$$K_{AH} = [0.010630\,(\, h^2 / a_{t-2}\,) - 0.010994(\, h^2_{t-1} / a_{t-2}\,)] + [53.695/h - 92.342/h_{t-1} + 40.090/h_{t-2} - 0.087996\, h^2_{t-2}\,]\, a^2_{t-1} + 0.10636\, a_{t-1}\, h_{t-2}$$

$$K_K = [\,-0.0000040479/\,(k_{t-1}\, k_{t-2}\,)\,]$$

Figure 8 presents the measured (solid line), fit (dotted line) and predicted (dashed line) shore-parallel current component. The fitted nonlinear model, spanning the first 150 hours (day 12.75 to 19.0) of the time series, is able to resolve to a reasonable degree most of the peaks contained within the shore-parallel current record. The fit does quite well in resolving the strong southerly directed flow between day 16.5 and 17.5, only missing the magnitude of the initial strong spike in velocity. The predicted shore-parallel current over the final 36 hours (day 19.0 to 20.5) of the time series indicates that the model is able to predict the overall magnitude and direction of the current but loses some of the higher resolution peaks contained in the data.

A determination of the dominant terms in equation 6 can be obtained by comparing the contribution of each forcing term utilized to fit the shore-parallel current component. Figure 9 is a comparison plot of the contribution of each predictive term in equation 6 relative to one another. The four terms in the empirical equation are those terms which are a function of the wind velocity, K_W, rate of change of the wind velocity, K_{dW}, tidal elevation and wave amplitude, K_{AH}, and the wave number, K_K. Examining Figure 9a and 9c, it is apparent that the dominant tidal structure of the predicted current velocity during these periods is driven by K_{AH}, the terms containing both the change in water surface elevation, h, and the wave amplitude, a. Additionally, it is evident that the frequency of the forcing produced by the tidal elevation and wave amplitude terms increases during the time period of strong southerly-directed currents (Figure 9b). As Figure 10 indicates, the frequency distribution of the kinetic energy density associated only with the terms containing the variation of water depth, h, and the wave amplitude, a, verifies that the nonlinear interaction between the two parameters is responsible for the measured current variability at 0.16 cph. The relative contributions of the remaining terms in equation 6 (Figure 9) indicate that the predicted current is strongly modified by the magnitude and direction of the shore-parallel wind velocity term, which can be of equal or greater magnitude than the water depth and wave amplitude terms. The shore-parallel wind velocity and the water depth - wave amplitude terms combine to produce the strong southerly-directed currents observed during the period of increased waye height (see Figures 6 and 9b). These two predictive terms are slightly modified by the rate of change of the wind velocity and the wave number terms during the wave event.

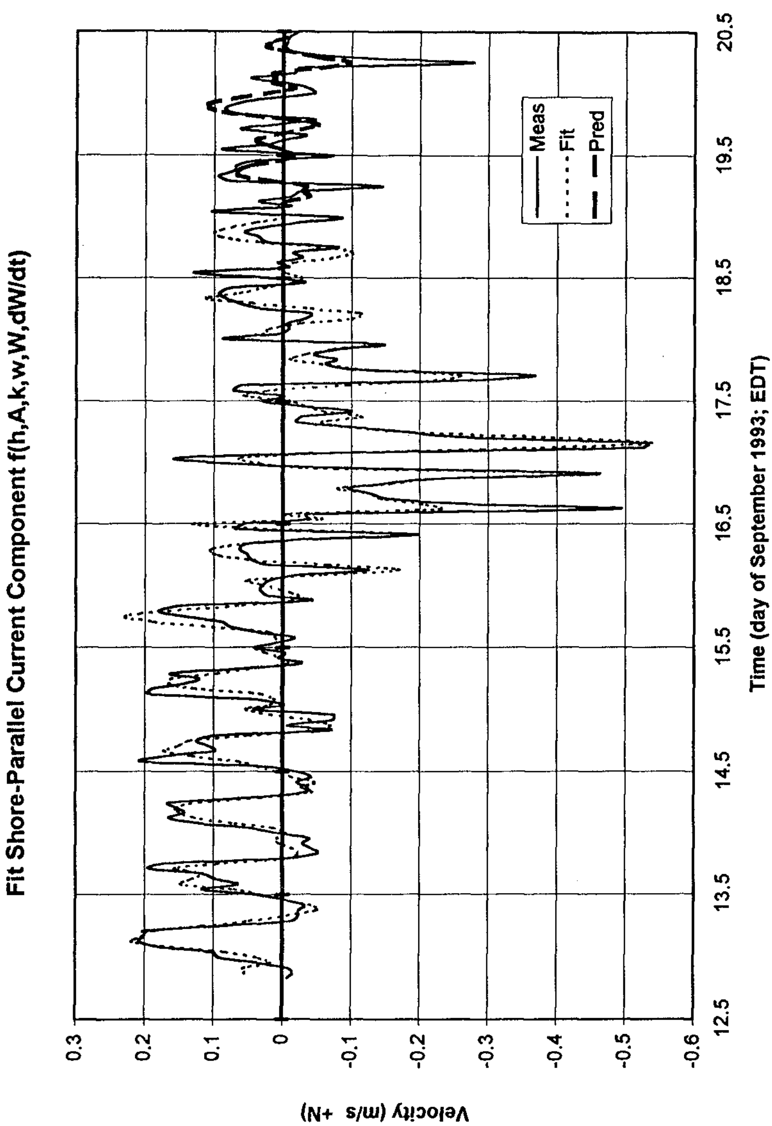

Figure 8. Empirical Fit of Measured Shore-Parallel Current

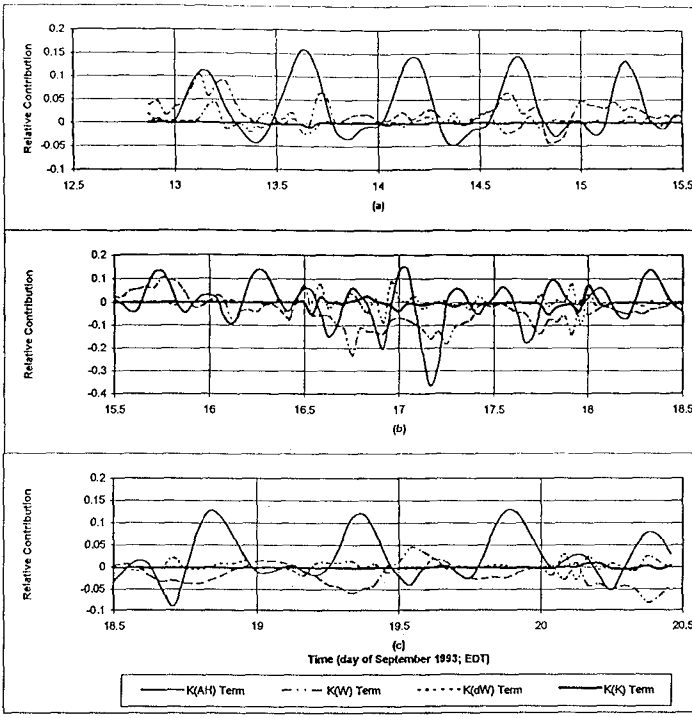

Figure 9. Relative Magnitude of Terms in Equation 6

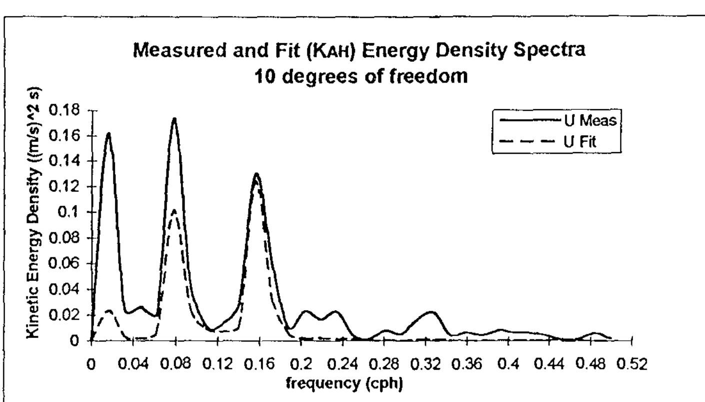

Figure 10. Influence of Water Depth and Wave Amplitude on Energy Distribution

Conclusions

Two tidal inlets with strikingly different physical characteristics have been investigated through an analysis of multi-year beach survey results and field investigations of the nearshore wave and current structure adjacent to the inlets. The downdrift shoreline adjacent to both inlets is dominated by persistent inlet directed currents, which run counter to the net sediment transport direction. The nearshore wave and current data obtained over a 8 day period at Townsends Inlet revealed that the nearshore current structure is dominated by inlet directed currents over both the flood and ebb tide. The empirical analysis of the measured data determined that an interaction between the wave climate and tide generate the observed inlet directed currents. However, strong episodic wind and wave events can reverse the observed current structure. The one day, high-resolution, wave and current study conducted at Manasquan inlet indicated a strong tidally-generated jet-like current exiting the inlet during ebb and persistent inlet-directed nearshore currents 550 m north of the inlet. A simplistic order of magnitude analysis of the measured data indicated that the potential motion induced by an ebbing tidal jet, and/or the wind-generated current contribute significantly to the observed current structure.

Although the characteristics of the two inlets differ, the hydrodynamic forcings are quite similar. Entrainment into the ebbing tidal jet leads to prolonged inlet directed nearshore currents updrift and downdrift of the inlet. The prolonged flood currents result in the reversal of the net alongshore current direction downdrift of the inlet, resulting in the formation of hot spots of erosion at the nodal points. The incident wind and wave forcing can be of equal magnitude to the potential flow generated by the tide, leading to episodic enhancement or reversal to the predominant flow characteristics.

Acknowledgements The authors wish to acknowledge the efforts of numerous individuals who assisted in the conduct of the field studies, including S. Glenn, R. Chant, and E. Creed from Rutgers University; and R. Hires and the numerous graduated students from Stevens Institute of Technology.

References

Bruno, M.S., Yavary, M. and Herrington, T.O. (1998). The influence of a stabilized inlet on adjacent shorelines: Manasquan, New Jersey, *Shore and Beach,* 66(2), 19-25.

Farrell, S.C., Sullivan, B. and Hafner, S. (1995). Annual report for 1994 to the borough of Avalon on the condition of municipal oceanfront and inlet beaches, 24pp., Coastal Research Center, Richard Stockton College of New Jersey.

Herrington, T.O. and Bruno, M.S. (1998). Empirical techniques for a priori parameter estimation, Estuarine and Coastal Modeling, Proceedings of the 5th International Conference, Alexandria, VA., Oct. 22-24, 1997, ASCE, 323-337.

Joshi, P.B. and Taylor, R.B. (1983). Circulation induced by tidal jets, *J. Wtrwy., Port, Coast., and Ocean Engrg.,* ASCE 109(4), 445-464.

Longuet-Higgins, M.S. (1970). Longshore currents generated by obliquely incident sea waves, 2, *J. Geophys. Res.,* 75(33), 6790-6801.

Pond, S. and Pickard, G.L. (1983). *Introductory Dynamical Oceanography, 2nd ed.* Pergamon Press, Inc., Maxwell House, Fairview Park, Elmsford, NY 10523.